BIOCHEMISTRY
including biophysical chemistry & molecular biology
Article

Biochemistry **2010,** *49,* 4601–4610 4601
DOI: 10.1021/bi901711w

Role of Juxtamembrane and Transmembrane Domains in the Mechanism of Natriuretic Peptide Receptor A Activation[†]

Marie Parat,[‡] Jonathan Blanchet,[§] and André De Léan*[,‡]

[‡]*Department of Pharmacology and* [§]*Molecular modeling platform of GÉPROM, Faculty of medicine, Université de Montréal, Montreal, Quebec, Canada H3T 1J4*

Received October 2, 2009; Revised Manuscript Received March 8, 2010

ABSTRACT: Natriuretic peptide receptor A (NPRA) is a noncovalent homodimeric receptor, composed of an extracellular domain (ECD) with a ligand-binding site, a single transmembrane domain (TM), and an intracellular domain (ICD) exhibiting guanylyl cyclase activity. NPRA activation by atrial natriuretic peptide (ANP) leads to cGMP production, which plays important roles in cardiovascular homeostasis. Initial studies have shown that activation of NPRA involves a conformational change in the juxtamembrane domain (JM). However, crystallographic study of the soluble ECD of NPRA has failed to document JM structure, and the conformational change involved in transmembrane signal transduction is still unknown. To analyze this conformational change, we first sequentially substituted nine amino acids of the JM with a cysteine residue. By studying the mutant's capacity to form ANP-induced or constitutive covalent disulfide dimers, we evaluated the relative proximity of JM residues, before and after NPRA activation. These results obtained with the full-length receptor demonstrate a high proximity of specific JM residues and are in disagreement with crystallography data. We also tested the hypothesis that signal transduction involves a TM rotation mechanism leading to ICD activation. By introducing one to five alanine residues into the TM α-helix, we show that a TM rotation of 40° leads to constitutive NPRA activation. We finally studied the role of the TM in NPRA dimerization. By using the ToxR system, we demonstrate that the last JM residues are required to stabilize the TM dimer. Using these experimental data, we generated a new molecular model illustrating the active conformation of NPRA, where the JM and TM are depicted.

Natriuretic peptides play a key role in cardiovascular homeostasis. Atrial natriuretic peptide (ANP)[1] and brain natriuretic peptide (BNP) are released by the heart in response to cardiac overload. Their physiologic effects include diuresis and natriuresis, inhibition of the renin−angiotensin−aldosterone system, and vasorelaxation, leading to a global decrease in blood pressure (*1*). They also serve a local protective role by preventing cardiac fibrosis and hypertrophy (*2*). Their physiologic role was exemplified in knockout mice with abrogated or reduced expression of ANP and BNP or their receptor NPRA which displayed hypertension, cardiac hypertrophy, and ventricular fibrosis (*3*). Cardioprotective properties of natriuretic peptides are used in therapeutic strategies. Indeed, Anaritide and Neseritide, ANP and BNP analogues, respectively, are currently used in the treatment of myocardial infarction (*4*, *5*). Currently, natriuretic peptide chimeras, like CD-NP and CU-NP, are being investigated to improve therapeutic efficacy and minimize undesirable effects in the treatment of acute decompensated heart failure (*6*, *7*).

Cellular effects of ANP are mediated through the transmembrane natriuretic peptide receptor A (NPRA). NPRA displays a typical particulate guanylyl cyclase structure with four structural domains: an extracellular domain (ECD) with a ligand binding site, a single transmembrane domain (TM), a kinase-like homology domain (KHD), and a guanylyl cyclase domain (GC), responsible for cGMP production (*8*). ECD specifically binds ANP in a 2:1 stoichiometric ratio (*9*), inducing a conformational change transmitted to the cytoplasmic domain through the TM. The KHD allosterically regulates both peptide binding to the ECD and activation of the GC (*10*, *11*). It is thought to maintain the receptor in the basal state, because receptors lacking this domain are constitutively active (*12*). The KHD responds to ANP binding by adopting a conformation that allows direct ATP binding, resulting in the release of the guanylyl cyclase activity repression (*13*). The KHD is also normally phosphorylated, and its dephosphorylation coincides with desensitization of NPRA to ANP activation (*1*, *14*). The GC domain presents two functional and allosterically regulated catalytic sites whose structure is jointly contributed by both subunits (*15*).

[†]This work was supported by Grant 13753 for the Canadian Institutes of Health Research.

*To whom correspondence should be addressed: Department of Pharmacology, Faculty of Medicine, Université de Montréal, 2900 boulevard Édouard-Montpetit, Pavillon Principal, V437-1, Montréal, Québec, Canada H3T 1J4. Telephone: (514) 343-6931. Fax: (514) 343-2291. E-mail: delean@pharmco.umontreal.ca.

[1]Abbreviations: A71915, (Arg[6], β-cyclohexyl-Ala[8], D-Tic[16], Arg[17], Cys[18])-rANP-(6−18)-amide; ANP, atrial natriuretic peptide; rANP, rat ANP; BNP, brain natriuretic peptide; CD-NP, full-length 22-amino acid human C-type natriuretic peptide (CNP) fused to the 15-amino acid carboxyl-terminal tail of *Dendroaspis* natriuretic peptide; CU-NP, ring structure and disulfide bond of CNP in combination with the N-terminus and the C-terminus of urodilatin; ECD, extracellular domain; EGFR, epidermal growth factor receptor; EpoR, erythropoietin receptor; ErbB2, epidermal growth factor receptor-2; FRET, fluorescence resonance energy transfert; GHR, growth hormone receptor; GC, guanylyl cyclase domain; GpA, glycophorin A; IBMX, 3-isobutyl-1-methylxanthine; ICD, intracellular domain; ΔICD, NPRA lacking its ICD; IGF-1R, insulin growth factor-1 receptor; IPTG, isopropyl β-thiogalactoside; JM, juxtamembrane domain; KHD, kinase homo logy domain; NMR, nuclear magnetic resonance; NPRA, natriuretic peptide receptor A; rNPRA, rat NPRA; PAGE, polyacrylamide gel electrophoresis; TM, transmembrane domain; WT, wild type.

Published on Web 03/09/2010

The juxtamembrane region (JM) connecting the bilobed ECD to the TM seems to play a crucial role in the transmembrane signal transduction mechanism. Indeed, it has been reported that ANP activation increases the protease sensitivity of the juxtamembrane region (*16*). Mutation C423S, which disrupts a short intrachain juxtamembrane disulfide-bridged loop, leads to both constitutive activation and receptor covalent dimerization through the exposed and unpaired C432 (*17*). This activation was later attributed to the conformational change induced by the loop disruption more than to the covalent dimerization process, because a C423S/C432S double mutation was shown also to be constitutively active but not covalently dimeric (*16*). However, the occurrence of a constitutive disulfide bridge still indicated the proximity of the juxtamembrane regions in the NPRA dimer. Moreover, mutation D435C, exposing a free cysteine three residues downstream of C432, led to an agonist-induced covalent dimer, indicating that a conformational change, either a translation or a rotation of the subunits, is occurring upon activation by ANP (*18*). Finally, fluorescence resonance energy transfer (FRET) studies with the ECD NPRA derivatized at C423 demonstrated that the ECD was spontaneously dimeric in solution, indicating that dimerization is not sufficient for NPRA activation. These studies also suggested that ANP and the antagonist A71915 both stabilize an ECD dimer form in which the juxtamembrane regions are in the proximity of each other, but in different conformations, supporting the hypothesis that the JM conformation determines the activation state of NPRA (*19*).

Crystallographic studies of the soluble liganded or unliganded extracellular domain of NPRA have failed to document the juxtamembrane domain structure and to identify the conformational change involved in signal transduction (*20*). The proper conformation of this region is probably dependent on its anchorage in the plasma membrane. For the single-transmembrane cytokine and tyrosine kinase receptors, one prevalently proposed activation mechanism involves subunit rotation within a receptor dimer (*21*−*24*). In the report presented here, we studied by cysteine scanning the JM conformation in a full-length receptor context. This method allowed us to evaluate the relative proximity of JM residues before and after NPRA activation. We then assessed by alanine insertion the hypothesis that signal transduction might involve a TM rotation mechanism. Alanine residues were inserted at the end of the TM. Indeed, each alanine insertion mimics a 100° rotation of the NPRA subunits. We also studied the role of the TM in NPRA dimerization using a bacterial ToxR assay for TM dimerization and demonstrated that the last residues of the JM stabilize the TM dimer. Finally, our data allow us to propose a new molecular model for NPRA's active conformation in which JM and TM regions are taken into account.

MATERIALS AND METHODS

Construction of NPRA Mutants. A wild-type rat NPRA clone inserted into pBK-CMV (Stratagene) between sites NheI and KpnI (pBK-NPRA) (*25*) was used for generating the various mutants. Nucleotide positions are numbered from the NheI insertion site. First, the BamHI site at position 1281 was eliminated by site-directed mutagenesis according to the Quikchange strategy (Stratagene). New BamHI and SpeI sites were created at positions 1421 and 1469, respectively, using mutagenic primers. The cysteine mutants were then obtained by ligating complementary pairs of oligonucleotides containing a cysteine substitution between the BamHI and SpeI sites. WT and cysteine mutant sequences between NheI and KpnI were then subcloned into the pcDNA5-FRT vector (Invitrogen). For the alanine mutants, a second SpeI site was created by site-directed mutagenesis at position 1547. The alanine mutants were obtained by ligating synthetic DNA linkers containing alanine insertions between the two SpeI sites. Synthetic DNA linkers were obtained by hybridization of five oligonucleotides. The ΔICD mutants lacking the cytoplasmic domain were obtained by PCR amplification of the cysteine mutants subcloned into the pcDNA5-FRT vector. The amplified fragment included the extracellular and transmembrane domains followed by the GERGSSTRG epitope, a stop codon, and finally a KpnI site. The ΔICD mutants sequences between EcoRI and KpnI were then subcloned into pBK-rNPRA.

Cell Culture. Human embryonic kidney cell line 293 (HEK293, American Type Culture Collection) was grown in Dulbecco's modified Eagle's medium (DMEM) supplemented with 10% fetal bovine serum and 100 units of penicillin/streptomycin in a 5% CO_2 incubator at 37 °C. The Flp-In-293 cells (Invitrogen) were grown in DMEM supplemented with 10% fetal bovine serum, 2 mM L-glutamine, 100 μg/mL zeocin, and 100 units of penicillin/streptomycin in a 5% CO_2 incubator at 37 °C.

Stable Expression in Flp-In-293 Cells. Transfection assays were conducted in 100 mm plates (1.2×10^6 cells) using calcium phosphate precipitation. Cells were cotransfected with pcDNA5-FRT vectors containing WT rNPRA or cysteine mutants and pOG44 plasmid [20 μg of total DNA/plate with a 9:1 (w/w) ratio of pOG44 to pcDNA5-FRT plasmids]. Clones were selected with 200 μg/mL hygromycin B in culture medium and tested for zeocin sensitivity according to the manufacturer's recommendations.

Transient Expression in HEK293 Cells. Transfection assays were conducted in 100 mm plates (1.2×10^6 cells) using calcium phosphate precipitation. Cells were transfected with 20 μg of total DNA/plate of pBK-rNPRA WT or alanine mutants and ΔICD mutant constructs.

Dimerization Assay. Dimerization assays were performed in 100 mm plates when cells were at subconfluence. Cells stably expressing cysteine mutants or transiently expressing ΔICD mutants were washed twice with serum-free DMEM and incubated at 37 °C with or without 10^{-8} M rANP (Sigma-Aldrich) or 10^{-5} M A71915 (Bachem) in the same medium containing 0.5% bovine serum albumin. After a 30 min incubation, cells were washed with PBS containing 10 mM NEM to prevent further covalent dimerization, and membranes were prepared according to the technique described below.

Membrane Preparations. Membranes were prepared according to the method of Labrecque et al. (*17*). Essentially, cells were harvested after the dimerization assay and homogenized with a Polytron homogenizer in ice-cold buffer [10 mM Tris-HCl (pH 7.4), 1 mM EDTA, and protease inhibitors]. After centrifugation at 40000*g* for 30 min, the pellets were washed and finally resuspended in freezing buffer containing 50 mM Tris-HCl (pH 7.4), protease inhibitors, 1 mM $MgCl_2$, and 250 mM sucrose. For the dimerization assay, 10 mM NEM (Sigma) was added to all the buffers to prevent undesirable disulfide bridge formation. Membranes were then frozen in liquid nitrogen and kept at −80 °C until further use. The protein concentration was determined using the BCA protein assay kit (Pierce).

Immunoblot Analysis. Membrane protein samples (20−80 μg) were solubilized in Laemmli sample buffer without β-mercaptoethanol (nonreducing condition) and heated at 100 °C for 5 min. Electrophoresis was performed in a 7.5% polyacrylamide gel for the ΔICD mutants and a 5% polyacrylamide gel for the full-length NPRA mutants. Following electrophoresis, proteins were transferred to a nitrocellulose membrane (Bio-Rad). The receptor was detected using an affinity-purified antibody from a rabbit polyclonal antiserum raised against the C-terminus of rNPR-A (*17*). Specific signals were probed with horseradish peroxidase-coupled second antibody according to the ECL Plus Western blotting analysis system and analyzed with a Typhoon Imager (GE Healthcare Life Sciences).

Whole Cell Guanylyl Cyclase Stimulation. Cells stably expressing rNPRA WT and cysteine mutants were plated in 24-well cluster plates at a density of 10^5 cells/well and incubated 24 h prior to agonist stimulation. Cells transiently expressing rNPRA WT and alanine mutants were replated 48 h post-transfection. The cells were washed twice with serum-free DMEM and incubated at 37 °C in quadruplicate wells with or without 10^{-7} M rANP (Sigma-Aldrich) in the same medium containing 0.5% bovine serum albumin and 0.5 mM 1-methyl-3-isobutylxanthine. After incubation for 1 h (cysteine mutants) or 1.5 h (alanine mutants), the medium was collected, and the level of accumulated extracellular cyclic GMP was determined by a radio-immunoassay (*26*). Maximal guanylyl cyclase activity was assessed on the same cells that remained attached to the plate. Cells were solubilized in 25 mM HEPES (pH 7.4) with 50 mM NaCl, 10 mM theophylline, 2 mM IBMX, 10 mM creatine phosphate, 10 units of creatine kinase, 1 mM GTP, 4 mM $MnCl_2$, and 1% Triton X-100. After incubation for 10 min (cysteine mutants) or 30 min (alanine mutants) under agitation, reactions were stopped by addition of 110 mM zinc acetate followed by 110 mM sodium carbonate as described previously (*15*). After centrifugation at 12000*g* for 2 min, supernatants were radio-immunoassayed for cyclic GMP content. Triton/Mn treatment is known to stimulate maximally the enzymatic domain of particulate guanylyl cyclase in a manner independent of the receptor activation state (*27*). It was used to normalize cGMP production results for differing levels of mutant protein expression and variation of cell number in each well.

Construction of the ToxR Chimeras. Synthetic linkers encoding different fragments of the rNPRA TM [TM1 and TM2 (Figure 6A)] were inserted between the ToxR transcription activator and the *Escherichia coli* maltose binding protein (MalE) within the pToxRI GpA13 T87G plasmid (*28*) previously cut with NheI and BamHI. pToxRI GpA13 and pToxRI GpA13 G83A plasmids, displaying the WT and mutated glycophorin A (GpA) TM, respectively, between the ToxR and MalE proteins, were used as positive and negative controls, respectively. ToxR system plasmids were kindly provided by D. Langosch (Lehrstuhl für Chemie der Biopolymere, Department für biowissenschaftliche Grundlagen, Technische Universität München, Weihenstephaner Berg 3, Freising, Germany).

In Vivo Detection of TM Homodimerization. Plasmids containing various ToxR chimera constructs (TM1, TM2, GpA, and GpA G83A) were transformed into *E. coli* FHK12 cells, which contain the β-galactosidase reporter gene. FHK12 cells were grown for 24 h at 37 °C at 255 rpm in the presence of 2% maltose, 0.4 mM IPTG, and 30 μg/mL chloramphenicol. β-Galactosidase activity was quantified in crude cell lysates after incubation at 37 °C for 20 min with *o*-nitrophenyl galactoside as described previously (*29*). The reaction was stopped with 90 μL of 1 M Na_2CO_3, and OD_{405} was measured using a microtiter plate reader. β-Galactosidase activity was measured in Miller units [1000(OD_{405} per minute)/OD_{600}].

ToxR Chimera Protein Expression Levels. Western blot analyses were performed with the FHK12 cells expressing the various ToxR chimera constructs used in the β-galactosidase activity assay. Aliquots of cells were mixed with sample buffer and boiled for 5 min. The samples were separated via a 10% SDS−polyacrylamide gel and then transferred to a nitrocellulose membrane (Bio-Rad). Detection of ToxR chimera constructs was achieved using a monoclonal anti-maltose-binding protein antibody (Sigma-Aldrich). Specific signals were probed with a horseradish peroxidase-coupled anti-mouse polyclonal antibody using the ECL Western blotting Analysis System (GE Healthcare Life Sciences).

Maltose Complementation Assay. Membrane insertion and correct orientation of the various ToxR chimera constructs (TM1, TM2, GpA, and GpA G83A) were examined as described previously (*30*). Briefly, PD28 cells were transformed with the different plasmids and cultured overnight. The cells were then washed twice and resuspended in phosphate-buffered saline and used to inoculate M9 minimal medium containing 0.4% maltose as the only carbon source. The time course of cell growth was measured at different time points with a spectrophotometer at 600 nm.

Molecular Modeling of the ECD and TM of NPRA in an Active Conformation. First, the model of the TM was obtained by homology modeling performed with the default parameters of Modeler 9v3 (*31*). The NMR structure of the dimeric transmembrane domain of the growth factor receptor ErbB2 was used as the template [Protein Data Bank (PDB) entry 2JWA] (*32*). Sequence alignment of the ErbB2 and NPRA TM was performed with 3D-COFFEE (*33*) (Figure 7A). Fifty models were created, and the lowest-energy one was chosen for the next step of modeling. The second step was to merge residues 423−435, which form a disulfide bridge loop, with the structure of the ECD NPRA−ANP complex (PDB entry 1T34) (*20*). These residues were indeed crystallized in the apo form of ECD NPRA (PBD entry 1DP4) (*34*). Their spatial conformation was merged with the ECD NPRA−ANP complex using ZMM (www.zmmsoft.com). Main chain atoms of residues 423−435 of the complex and the same residues of the loop were superimposed using energy minimization and distance constraints of 0 Å for homologous atoms. No major conformational changes were observed during the minimization process. A similar energy minimization protocol was used to merge the TM with the ECD NPRA−ANP complex. Merging involved residues 433−435 of the main structure and the same residues of the TM helices, and only residues 421−437 had freedom of movement during the minimization. At this point, the structure was complete (ECD and TM). The last step of the modeling was to impose a proximity constraint between the D435 residues from both subunits to suit experimental results. We used many molecular dynamics and relaxation steps until the distance between the C_α atoms of the residues was no more than 7 Å. Module Discover3 of InsightII (Accelrys) was used for all the dynamic simulations, with the CVFF force field and a shell of explicit water molecules of 8 Å. During all the simulations, the backbone of the complex was tethered to its original position, except for residues 422−437 inclusively.

Data Analysis and Statistics. Guanylyl cyclase activities were analyzed with RiaFit, which was based on the

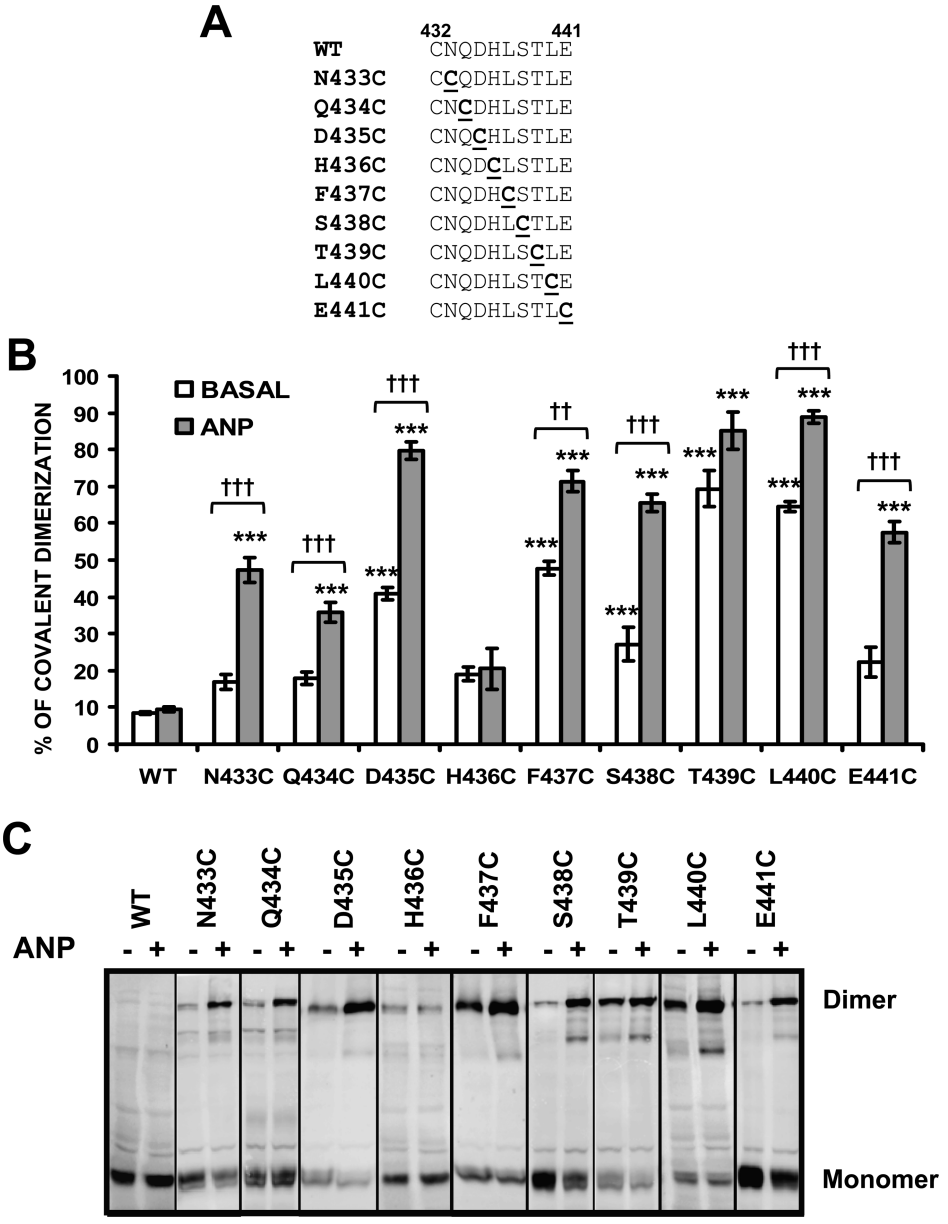

FIGURE 1: Covalent dimerization of NPRA cysteine mutants. (A) Site-directed mutations in the NPRA JM. The cysteine substitutions are underlined. (B) Covalent dimerization levels of cysteine mutants. Flp-In-293 cells stably expressing WT NPRA or cysteine mutants were untreated (white) or treated (gray) with 10^{-8} M rANP at 37 °C for 30 min. Membranes (20−80 μg) prepared from these cells in the presence of NEM (to prevent nonspecific covalent dimerization) were loaded onto a nonreducing 5% SDS−PAGE gel. Receptor monomers and covalent dimers were detected by Western blotting using a specific antibody as described in Materials and Methods and analyzed with a Typhoon Imager. For each mutant, levels of receptor dimers and monomers were measured by densitometry with ImageQuant TL v2005 and were used to calculate covalent dimerization percentages. $N = 4-12$. $P < 0.01$ (two asterisks) and $P < 0.001$ (three asterisks) compared to the WT. $P < 0.01$ (two daggers) and $P < 0.001$ (three daggers) compared to the basal level of covalent dimerization. (C) Representative examples of Western blots of the cysteine mutants with or without ANP.

four-parameter logistic equation (*35*). Statistical testing of repeat experiments was performed by analysis of variance, followed by a post hoc Dunnett's test, with a $p < 0.05$ significance level.

RESULTS

Evaluation of the Relative Proximity of the JM Residues within the NPRA Dimer. The NPRA JM plays a critical role in receptor activation (*17*, *18*). To analyze the ANP-induced conformational change in the JM, we sequentially substituted the nine amino acids of the JM with a cysteine residue (Figure 1A). By studying the mutant's ability to form ANP-induced or constitutive covalent disulfide dimers, we evaluated the relative proximity of JM residues, before and after NPRA activation. Indeed, the ability to form a disulfide cross-link implies that the JM residues are closely apposed in the receptor dimer (~7 Å between the C_α atoms). To determine whether these mutants, when stably expressed in Flp-In-293 cells, could form intermolecular disulfide bonds, we performed nonreducing SDS−PAGE and Western blotting and measured the percentage of covalent dimerization by densitometry (Figure 1C).

We first performed saturation binding assays to verify that WT and cysteine mutants had similar affinity for ANP and similar expression levels. Indeed, the pK ($= -\log K_d$) for ANP binding was maintained between 11.0 and 11.4, and the receptor expression level was between 1 and 3.0 pmol/mg (data not shown).

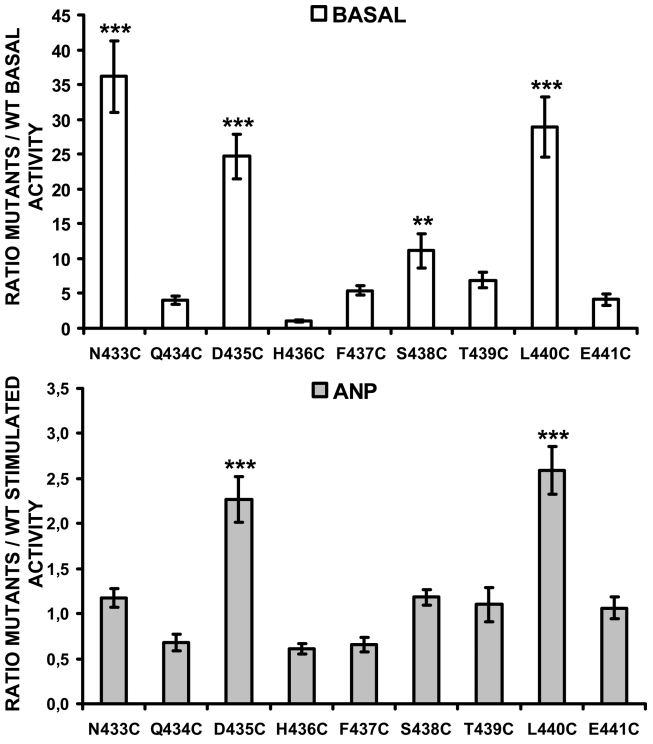

FIGURE 2: Guanylyl cyclase activity of NPRA cysteine mutants. Flp-In-293 cells stably expressing WT NPRA or cysteine mutants were untreated (white) or treated (gray) with 10^{-7} M rANP at 37 °C for 1 h, as described in Materials and Methods. The level of cGMP accumulation was measured in the extracellular medium by radioimmunoassay. Results were normalized according to the maximal activation level of solubilized cells obtained in Triton and Mn^{2+}. The results are expressed as a ratio of mutant to WT NPRA activity under basal conditions (white) or after stimulation by ANP (gray). $N = 4-12$. $P < 0.01$ (two asterisks) and $P < 0.001$ (three asterisks) compared to the WT.

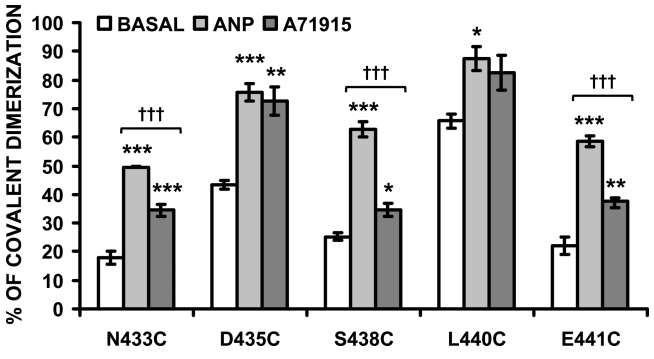

FIGURE 3: Effect of antagonist A71915 on the covalent dimerization of NPRA cysteine mutants. Flp-In-293 cells stably expressing WT NPRA or cysteine mutants were untreated (white) or treated with 10^{-8} M rANP (gray) or 10^{-5} M A71915 (dark gray) at 37 °C for 30 min. Membranes (20−80 μg) prepared from these cells in the presence of NEM (to prevent nonspecific covalent dimerization) were loaded on a nonreducing 5% SDS−PAGE gel. Receptor monomers and covalent dimers were detected by Western blotting using a specific antibody as described in Materials and Methods and analyzed with a Typhoon Imager. Levels of receptor dimers and monomers were measured by densitometry with ImageQuant TL v2005 and were used to calculate covalent dimerization percentages. $N = 3$. $P < 0.01$ (two asterisks) and $P < 0.001$ (three asterisks) compared to the basal level of covalent dimerization. $P < 0.01$ (two daggers) and $P < 0.001$ (three daggers) compared to the ANP-induced level of covalent dimerization.

In the basal state, only some mutants are able to efficiently form covalent dimers (Figure 1B), especially T439C and L440C, which are 70 and 65% dimeric, respectively. However, upon binding by ANP, almost all the mutants are able to dimerize with variable efficiency. In particular, the extent of dimerization is very high (> 60%) for D435C and F437C to L440C. These results suggest that the JM conformation is constrained in the basal state and becomes more flexible upon ANP binding. In addition, ANP seems to induce repositioning of the JM residues. This is particularly true for D435C, S438C, and E441C which display a large induction of dimerization by ANP (> 2-fold higher than the basal level).

Dimerization Is Necessary but Not Sufficient for NPRA Activation. To determine if residue proximities observed above were characteristic of the basal or active state of the NPRA, we measured the guanylyl cyclase activity of cysteine mutants in the basal state and after ANP stimulation. The amount of accumulated cGMP in extracellular medium was measured and normalized using the maximal activity measured after Triton/Mn solubilization of cells remaining attached in wells.

As indicated in Figure 2, some mutants are constitutively active in the basal state, in particular N433C, D435C, and L440C which have guanylyl cyclase activities 36-, 25-, and 29-fold higher than that of WT NPRA, respectively. However, the level of the disulfide-linked dimer is not correlated with the extent of guanylyl cyclase activity. For example, T439C shows the strongest extent of dimerization in the basal state, with almost 70% of the total cellular receptor as a disulfide-linked dimer (Figure 1B), but exhibits a guanylyl cyclase activity similar to that of WT NPRA (Figure 2). On the other hand, the L440C mutant, which shows the next highest percentage of dimerization in the basal state [65% (Figure 1B)], is constitutively active. Intriguingly, N433C is constitutively active in the basal state, with the highest guanylyl cyclase activity of all, although it was unable to form an interchain disulfide bridge in this basal state (Figure 1B). This increase in guanylyl cyclase activity could be due to the mutation itself. Indeed, the Asn substitution by a more hydrophobic amino acid could change the juxtamembrane conformation. In addition, in the N433C mutant, the additional cysteine is located just next to cysteine 432 which is involved in the intrachain C423−C432 loop. It has been demonstrated that an alteration of this loop, by the C423S/C432S mutation, leads to a constitutive activation of NPRA without disulfide bridge formation (*16*). The formation of an altered C432−C433 loop with an extra amino acid in the N433C mutant could explain its high constitutive activity.

D435C and L440C, which were constitutively active in the basal state, are also almost 2.5-fold more active than WT NPRA in the presence of ANP. As these mutants were highly covalently dimeric in the presence of ANP, we can suggest that the proximity of D435 and L440 residues within the NPRA dimer is crucial for NPRA activation.

In a previous publication (*19*), we suggested that dimerization was not sufficient for NPRA activation by demonstrating that the antagonist A71915 stabilizes a dimeric form of ECD NPRA. We next used the cysteine mutants to confirm this suggestion. We compared the ability of the antagonist A71915 and agonist ANP to induce covalent dimerization of some cysteine mutants. All mutants exhibited some increase in the level of covalent dimerization with each ligand, but we observed that N433C, S438C, and E441C mutants exhibited different profiles of covalent dimerization according to the ligand (Figure 3). Results indicate that the antagonist A71915 stabilizes a dimeric form of the

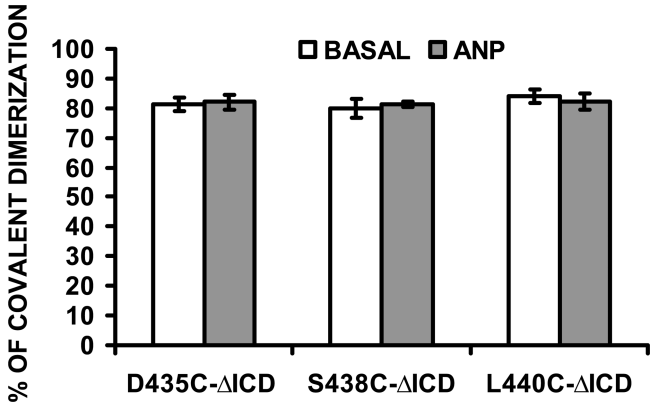

FIGURE 4: Covalent dimerization of NPRA cysteine mutants lacking their ICD. HEK293 cells transiently expressing ΔICD cysteine mutants were untreated (white) or treated (gray) with 10^{-8} M rANP at 37 °C for 30 min. Membranes (20−80 μg) prepared from these cells in the presence of NEM (to prevent nonspecific covalent dimerization) were loaded on a nonreducing 7.5% SDS−PAGE gel. Receptor monomers and covalent dimers were detected by Western blotting using a specific antibody as described in Materials and Methods and analyzed with a Typhoon Imager. Levels of receptor dimers and monomers were measured by densitometry with ImageQuant TL v2005 and were used to calculate covalent dimerization percentage. $N = 3$.

NPRA in which the JM residues are in a conformation different from those of the active and basal states.

Even though the positioning of N433, S438, and E441 seems to be discriminating, D435C and L440C exhibit the same covalent dimerization profiles with A71915 and ANP (Figure 3). One can speculate that this observation contradicts our conclusion that the proximity of D435 and L440 is crucial for NPRA activation. However, the antagonist A71915 is in fact a weak partial agonist (*36*). The proximity of D435 and L440 residues induced by A71915 could be responsible for its partial agonist activity.

We can conclude that dimerization is clearly not sufficient for NPRA activation. The receptor activation is not accomplished simply by bringing two receptor subunits into the proximity of one another. Thus, the relative orientation of the two juxtamembrane domains of the NPRA dimer, rather than their proximity, determines the activation state of the receptor.

The Intracellular Domain Imposes a Conformational Constraint on the JM in the Basal State. Our next objective was to assess the potential role of the intracellular domain in the conformational constraint observed in the basal state in the cysteine mutant covalent dimerization studies. We thus obtained constructs with truncations of the whole intracellular domain on some cysteine mutants which displayed a high level of induction of dimerization by ANP, such as D435C and S438C, or a high percentage of covalent dimerization in the basal state, such as L440C.

Covalent dimerization of the ΔICD mutants appears almost complete in the basal state (80%), whereas it was less elevated for full-length D435C, S448C, and L440C mutants (41, 27, and 65%, respectively). Furthermore, ANP has no further effect on the dimerization level (Figure 4). Therefore, the intracellular domain is responsible for the JM conformational constraint observed in the basal state.

Constitutive NPRA Activation by Relative Subunit Rotation. Previous studies in our laboratory demonstrated that dimerization of NPRA is not sufficient for activation (*19*). These results have been confirmed in this study. Furthermore, the

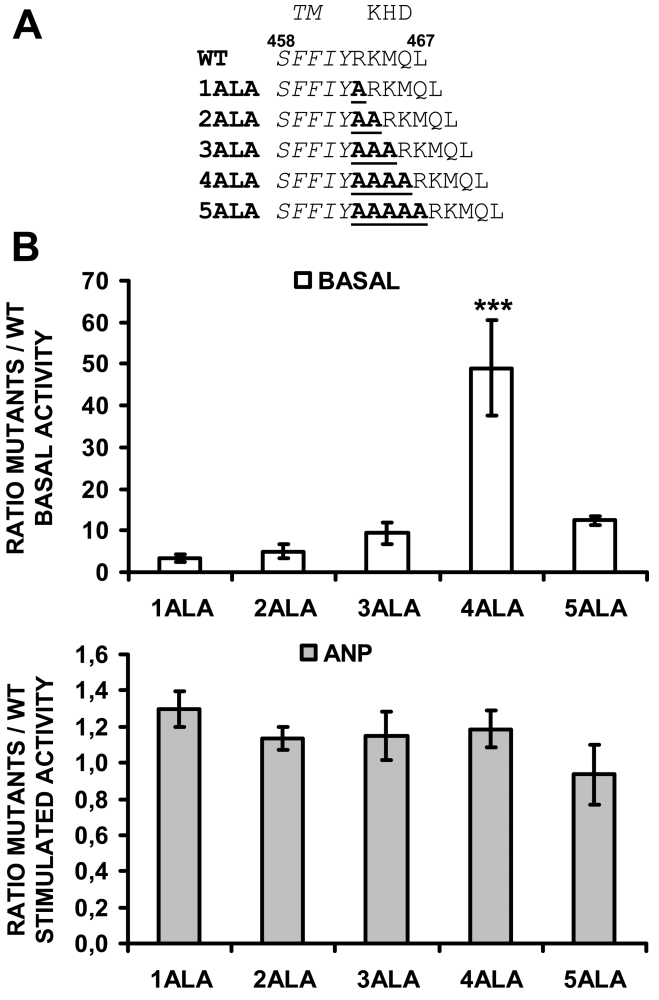

FIGURE 5: Effect of subunit rotation on NPRA guanylyl cyclase activity. (A) Alanine residues (underlined) were sequentially introduced at the end of the TM after Y462 (italicized). (B) Guanylyl cyclase activity of NPRA alanine mutants. HEK293 cells transiently expressing WT NPRA or alanine mutants were untreated (white) or treated (gray) with 10^{-7} M rANP at 37 °C for 1.5 h, as described in Materials and Methods. The level of cGMP accumulation was measured in the extracellular medium by radio-immunoassay. Results were normalized according to the maximal activation level of solubilized cells obtained in Triton and Mn^{2+}. The results are expressed as a ratio of mutant to WT NPRA activity under basal conditions (white) or after stimulation by ANP (gray). $N = 5$. $P < 0.001$ compared to the WT (asterisks).

minor extent of conformational difference between the unliganded and liganded forms of the ECD illustrated by crystallography restricts options for transmembrane signaling (*20*). We thus tested the rotation mechanism hypothesis by introducing one to five alanine residues running from the TM α-helix (Figure 5A). Indeed, polyalanine peptides form α-helix structures in which each helix turn contains 3.5 amino acids so that each alanine insertion results in an ICD rotation of ~100° (360°/3.5).

Alanine insertion resulted in highly significant constitutive activity only in the case of the four-alanine insertion [~49-fold greater than WT activity (Figure 5B)]. This insertion is predicted to rotate the intracellular domain a total of 400°, thus 40° clockwise past the initial position. The five-alanine insertion does not induce a significant constitutive activation, indicating that constitutive activity depends on the degree of rotation and not on the number of alanines inserted. Because there is no sequential increase in activity with serial addition of alanine residues, a

piston mechanism can be excluded. Surprisingly, alanine insertion has no effect on ANP-induced activity, since alanine mutants exhibit the same induced activity as the WT receptor (Figure 5B). This observation could be explained by the fact that ANP binding increases flexibility in receptor conformation, as observed in the cysteine mutant dimerization assay. These results still support the hypothesis that TM helix rotation is a part of NPRA transmembrane signaling.

The Last Residues of the JM Stabilize the NPRA TM Dimer. Our studies of rNPRA cysteine mutants suggested a close proximity of some JM residues and the presence of a dimerization interface at the beginning of the α-helical TM segment. The orientation of the TMs in the plasma membrane and the role of these domains in NPRA dimerization have not been studied. We therefore used the simple and robust ToxR system to assess the ability of NPRA TMs to self-assemble in vivo (*28*). The ToxR transcriptional activator can be used successfully to assess weak TM−TM interactions within the *E. coli* membrane. TMs under study are inserted between a periplasmic maltose binding protein and a cytoplasmic ToxR transcription activator protein. Dimerization of the TMs in this system results in the association of the ToxR transcriptional activator, which can then activate the transcription of the *β*-galactosidase reporter gene. Quantification of the level of TM dimerization is then obtained by measuring the *β*-galactosidase activity.

To assess the role of the last residues of the JM in TM dimerization, we tested two constructs of the NPRA TM. TM1 displayed the last three residues of the JM and the first 13 residues of the TM. TM2 displayed only the first 16 residues of the TM (Figure 6A). We used the well-investigated self-interacting GpA TM as a positive control for homodimerization and the GpA G83A mutant which lacks the capacity to dimerize as a monomeric control (*28*).

We first verified the expression levels of all the chimeras and their proper insertion into the membrane by performing Western blotting and maltose complementation assays. The expression levels of the chimeras were similar for Neg, Pos, and TM1 (Figure 6B inset). Densitometric quantification of five independent blots established that average levels of these ToxR constructs range from 95% (TM1) to 125% (Pos) of the negative control (data not shown). The TM2 construct was however overexpressed [~200% of the negative control (data not shown)]. The membrane insertion and correct orientation of the various constructs were assessed via examination of the ability of the transformed PD28 bacteria, which lack the endogenous maltose-binding protein gene, to grow on minimal M9 medium containing maltose as the only carbon source. Indeed, these bacteria are unable to grow without the presence of a properly inserted chimera membrane protein. We followed the PD28 growth curve for 44 h. All constructs exhibited similar rates of cell growth (Figure 6C), indicating proper membrane integration. Thus, we conclude that all the constructs used in this study are expressed and inserted in the correct orientation into the inner membrane.

We then evaluated the *β*-galactosidase activity of our NPRA TM constructs to assess their capacity to dimerize. The TM2 construct exhibited a signal similar to the negative control, corresponding to a monomeric TM. The TM1 construct displayed a signal significantly higher than the negative control (~2.5-fold), indicating its propensity to dimerize (Figure 6B). These results demonstrate that the last three residues of the JM (T439, L440, and E441) are required to stabilize the TM dimer.

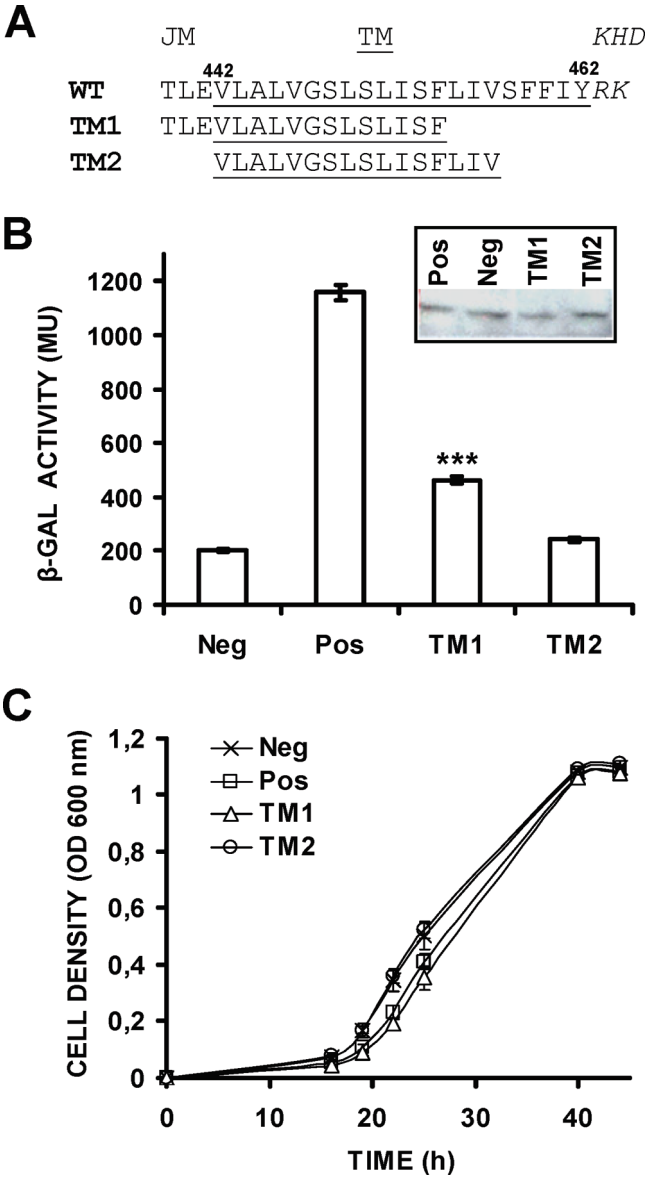

FIGURE 6: Homodimerization of NPRA TMs. (A) Amino acid sequences of two NPRA TM segments (TM1 and TM2) as expressed in the context of the ToxR system. NPRA TM residues are underlined. (B) *β*-Galactosidase activity of the NPRA TM chimeras. *β*-Galactosidase activity was quantified in crude lysates of FHK12 bacteria expressing the ToxR chimera as described in Materials and Methods. The GpA TM was used as a positive control for homodimerization (Pos) and GpA G83A mutant which lacks the capacity to dimerize as a monomer control (Neg). $N = 20-28$. $P < 0.001$ (asterisks) compared to the negative control (Neg). The inset shows the expression levels of the ToxR chimera proteins (70 kDa). FHK12 bacteria used in the *β*-galactosidase activity experiment resuspended in sample buffer were loaded on a 10% SDS−PAGE gel. ToxR constructs were detected using an anti-MBP antibody as described in Materials and Methods. The result is representative of five identical experiments. (C) Control for correct membrane integration. PD28 cells transformed with the ToxR constructs [Neg (×), Pos (□), TM1 (△), and TM2 (○)] were grown in minimal medium containing maltose as the only carbon source. The cell density as monitored by optical density at 600 nm (OD_{600}) at different time points reflects the efficiency of membrane integration. Each data point represents the mean ± standard error of quadruplicate determinations. The results are representative of three identical experiments.

These data furthermore reinforce the hypothesis of the proximity of the last juxtamembrane residues documented by cysteine mutant studies.

Active Conformational Model of NPRA. Crystallographic studies of the soluble liganded or unliganded extracellular domain of NPRA have failed to document the structure of the JM. The JM is poorly structured in solution, suggesting that its conformation is dependent on the TM and ICD domains. According to the ANP-liganded crystal, the NPRA extracellular domain subunits are composed of two well-structured lobes followed by a disulfide bridge loop (C423−C432) which links the JM to the lower lobe. Disulfide-bridged loops are hanging under the lower lobes with D435 residues of each subunit pointing in opposite directions (*20*, *34*). Our results are in disagreement with these crystallographic data, since we demonstrated that D435 residues are in close proximity of the activated state of NPRA. We thus generated an improved molecular model illustrating the active conformation of NPRA in which the TMs are taken into account.

We first built a model of the TM by homology modeling using the ErbB2 TM structure as a template. ErbB2 is a single-transmembrane receptor with the same topology as NPRA. Moreover, the RMN structure of the ErbB2 TM in an active conformation displayed a dimerization interface at the beginning of the TM (*32*), and our results suggested that it is also the case for NPRA. Finally, alignment of ErbB2 and NPRA TM amino acid sequences shows sufficient homology (Figure 7A). The resulting TM structure was then merged with the ECD crystal structure by energy minimization, and finally proximity constraints of C432 and D435 residues of the JM were imposed by molecular dynamics.

In contrast with the crystal structure, our proposed model shows that the disulfide-bridged loops C423−C432 are positioned horizontally under the lower lobes (Figure 7B). In addition, the two D435 residues are now in close proximity. The last three residues of the JM (T439, L440, and E441) are located in an outer extension of the transmembrane α-helix. These residues, as well as the initial residues of the TM, form a helix−helix interface, which is putatively mediating NPRA activation.

DISCUSSION

Ottemann et al. (*37*) postulated general models for transmembrane signaling based on hypothetical motions in the transmembrane region. Their models included association, dissociation, piston, rotation, scissor, and seesaw mechanisms. Until recently, the general consensus was that signaling by most single-transmembrane receptors occurs by an association mechanism, in which ligand binding brings the receptor molecules close together, and this proximity activates in turn the effector enzyme. However, many recent studies on cytokine and tyrosine kinase receptors contradicted this consensus and demonstrated that dimerization is required but not necessarily sufficient for receptor activation (*38*). First, many of these receptors are normally present as dimers on the surface of the cell in the absence of ligand (*21*, *23*, *39*, *40*). Moreover, certain covalently dimeric receptors, such as the A653C ErbB2 mutant or IGF-1 receptor, are inactive (*38*, *40*). Finally, antagonists also stabilize the dimeric form of some of these receptors, as shown for Epo receptor (EpoR) antagonist EMP33 (*41*). Activation of most single-transmembrane receptors thus seems to be orientation-dependent. NPRA is dimeric at the surface of the cell in the absence of ligand (*42*). We also recently demonstrated that ANP binds a preformed soluble ECD dimer of NPRA and that the antagonist A71915 also stabilizes a dimeric form of ECD (*19*). Taken together, these data clearly suggest that dimerization is insufficient for NPRA activation. Several studies have suggested that activation of NPRA involved a conformational change in the JM (*16*−*18*). Here, we confirm this hypothesis and demonstrate that the relative orientation of the two juxtamembrane domains of the NPRA dimer, rather than their proximity, determines the activation state of the receptor (Figures 1−3). Indeed, both the agonist and the antagonist stabilize a dimeric form of the NPRA where JMs occur in different conformations, which are distinct from that of the basal conformation.

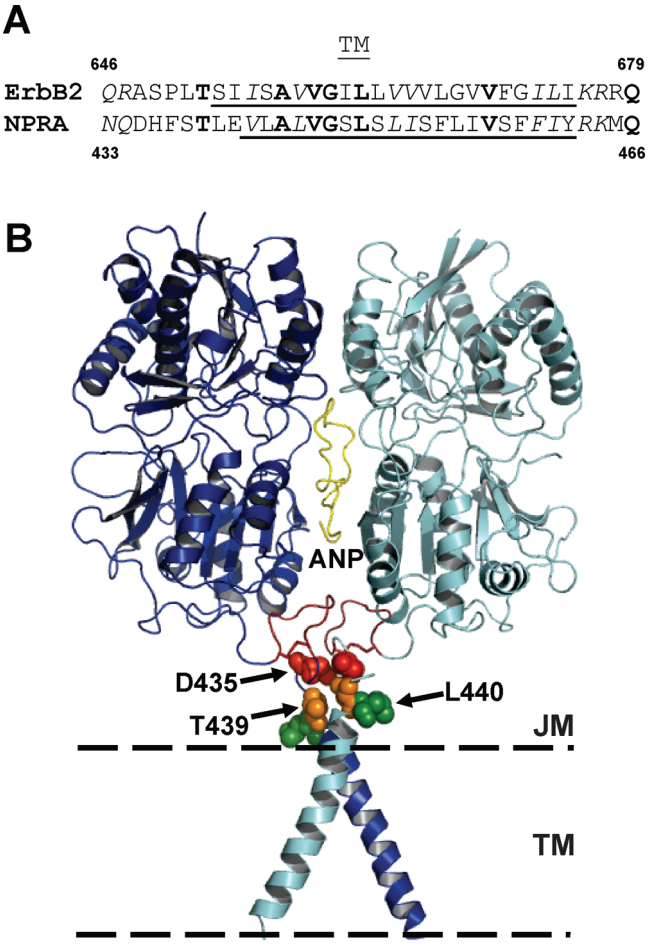

FIGURE 7: Model of the active conformation of the NPRA ECD and TM. (A) Amino acid sequence alignment of ErbB2 and the NPRA TM obtained with 3D-COFFEE. Identical residues are shown in bold, and homologous residues are italicized. Transmembrane residues are underlined. (B) Modeling of the rNPRA ECD and TM in complex with ANP was conducted as described in Materials and Methods. NPRA homodimer subunits (dark and light blue) and ANP (yellow) are shown in a ribbon model using PyMol. Disulfide bridge loops C423−C432 are colored dark red. JM residues expected to be in the proximity are indicated and shown in a sphere model [D435 (light red), T439 (orange), and L440 (green)]. The membrane double layer is shown as dashed lines.

Transmembrane signaling of some single-transmembrane receptors is likely to involve a rotational mechanism (*21*−*24*). The EpoR receptor seems to be activated by a combination of scissor movement and subunit rotation (*24*, *38*), whereas GH receptor (GHR) activation requires relative subunit rotation and vertical movement (*21*). A rotational mechanism has also been proposed for the EGF receptor (EGFR) and ErbB2 (*22*, *23*). We could expect that the conformational change induced by ANP on the ECD dimer would be much more subtle than conformational changes observed for growth hormone or cytokine receptors.

Indeed, cytokines are larger proteins that present a well-defined secondary structure in both free and receptor-bound states. In contrast, natriuretic peptides are small polypeptides with a disordered conformation in solution (*43*), and they must acquire a flat penny-like conformation by selection or induction when binding intercalated between the two ECD monomers of NPRA. Moreover, crystallographic studies showed a minor extent of conformational difference between the unliganded and liganded forms of the NPRA ECD, restricting options for transmembrane signaling mechanisms (*20*). Here, we tested the hypothesis of a rotational mechanism and demonstrated that a 40° rotation of the NPRA TM leads to a constitutively activated receptor, although not fully. It is noteworthy that GHR is also constitutively activated by a 40° rotation of the TM (*21*). However, the constitutive rotation-dependent activation of NPRA is partial compared to ANP activation (6% of the maximal ANP-activated level). The fact that rotation is not sufficient for full activation of the receptor suggests that rotation is not the sole mechanism involved in signal transduction. Alternatively, we cannot exclude the possibility that alanine insertion incompletely mimics transmembrane domain rotation for NPRA. We also demonstrated that proximity of certain JM residues is crucial for NPRA activation (Figures 1 and 2). Thus, we can hypothesize that signal transduction would involve a combination of subunit rotation together with additional translations which bring crucial residues of the JM into proximity.

We have originally proposed a rotational mechanism for NPRA activation based on the observation of agonist-induced covalent dimerization of the D435C mutant of full-length NPRA (*18*). Ogawa et al. confirmed this proposed rotational mechanism for NPRA soluble ECD, based on crystallographic study (*20*). However, this rotation mechanism is drastically different from the one that we propose here. In Ogawa's model, the proximity of JMs is not taken into account because they are absent from the structure documented. On the contrary, the central axes of the ECD subunits, including part of the JM, seem to move away from each other upon ANP binding. Although this structural study of the soluble ECD is certainly informative, it is not sufficient to describe the activation mechanism of NPRA in the context of the membrane-bound full-length receptor. Activation mechanisms must be studied in a full-length receptor context especially with NPRA, since mutual allosteric influences of ECD and ICD have been demonstrated. Indeed, as we are showing in this study, ICD constraints the JM conformation to the basal state (Figures 1 and 4). Agonists overcome this constraint, thus permitting initiation of activation (Figure 1). Following the response of the ICD to JM and TM conformational changes, ATP binds to the KHD, inducing guanylyl cyclase activation as well as an increased ANP dissociation rate (*10*, *11*).

Our model takes the JM and TM into account, and TMs are expected to influence ECD and particularly JM conformation (Figure 7). Accordingly, we demonstrated that T439, L440, and E441 residues are required and sufficient for the stabilization of the TM dimer (Figure 6). Moreover, we illustrated the proximity of these residues in the NPRA dimer by cysteine mutation studies (Figure 1). The TM of NPRA was predicted to begin with residue V442. However, our TM dimerization study suggests that T439, L440, and E441 residues are also part of the transmembrane α-helix. ErbB2 and NPRA sequence alignment suggests that L440 and E441 could be part of the transmembrane domain and that T439 would be the α-helix cap. The specific role of these three residues in the full-length receptor remains to be studied in detail. Our model illustrates the active state of NPRA and is the first model in which the JM and TM are depicted. Obviously, this model is represented as a snapshot image, whereas activation mechanisms are dynamic processes. Recent studies suggest the occurrence of multiple conformations for G-protein-coupled receptor activation. This concept suggests the existence of multiple, ligand-specific conformational states and multiple conformational intermediates between the basal and maximal activation states (*44*). This concept could be applied to single-transmembrane receptors. Indeed, it has been demonstrated using crystallography that the natural agonist Epo and mimetic agonist EMP1 induce very different conformational changes in EpoR (*38*). Likewise, our FRET studies with NPRA ECD showed that the conformation of ligand-bound dimers differs depending on the agonist bound (*19*). The traditional concept of dual active and inactive conformations is most likely an oversimplification of the receptor signal transduction mechanism that has now evolved into a more detailed kinetic model of signal transduction.

The NPRA activation process is currently divided into two steps. (1) ANP binding induces a conformational change in the JM, presumably transmitted through the membrane by a rotation of the TM. This rotation then allows ATP binding, perhaps by exposing the ATP binding site. (2) ATP binding induces another conformational change that is transmitted through the coiled coil connecting the KHD with the GC. Although the conformational changes occurring in the ICD remain to be elucidated, this could occur perhaps by an axial rotation or a lateral movement, which would then allow full activation of guanylyl cyclase. Crystallographic documentation of the structure of ICD should provide further insight into the signal transduction of NPRA. Here, we identified a plausible mechanism illustrating signal transduction through the cell membrane which could be applied to other membrane guanylyl cyclases and could contribute to an improved understanding of other single-transmembrane receptors. The generation of a full-length molecular model in the basal state would be also needed. Further studies will be required to document the dynamic conformational changes in the NPRA activation mechanism.

ACKNOWLEDGMENT

We greatly appreciate the gift of ToxR system vectors and bacterial strains from Dr. Dieter Langosch (Lehrstuhl für Chemie der Biopolymere). We are grateful to the GÉPROM (Groupe d'Étude des Protéines Membranaires) for allowing access to its molecular modeling platform. We thank Dr. Simon Joubert for critical reading of the manuscript.

REFERENCES

1. Potter, L. R., Abbey-Hosch, S., and Dickey, D. M. (2006) Natriuretic peptides, their receptors, and cyclic guanosine monophosphate-dependent signaling functions. *Endocr. Rev. 27*, 47–72.
2. Gardner, D. G., Chen, S., Glenn, D. J., and Grigsby, C. L. (2007) Molecular biology of the natriuretic peptide system: Implications for physiology and hypertension. *Hypertension 49*, 419–426.
3. Kuhn, M. (2004) Molecular physiology of natriuretic peptide signalling. *Basic Res. Cardiol. 99*, 76–82.
4. Strain, W. D. (2004) The use of recombinant human B-type natriuretic peptide (nesiritide) in the management of acute decompensated heart failure. *Int. J. Clin. Pract. 58*, 1081–1087.
5. Lee, C. Y., and Burnett, J. C., Jr. (2007) Natriuretic peptides and therapeutic applications. *Heart Failure Rev. 12*, 131–142.
6. Dickey, D. M., Burnett, J. C., Jr., and Potter, L. R. (2008) Novel bifunctional natriuretic peptides as potential therapeutics. *J. Biol. Chem. 283*, 35003–35009.

7. Lee, C. Y. W., and Burnett, J. C., Jr. (2007) Discovery of a Novel Synthetic Natriuretic Peptide, CU-NP. *J. Card. Failure 13*, S74.
8. Padayatti, P. S., Pattanaik, P., Ma, X., and van den Akker, F. (2004) Structural insights into the regulation and the activation mechanism of mammalian guanylyl cyclases. *Pharmacol. Ther. 104*, 83–99.
9. Rondeau, J. J., McNicoll, N., Gagnon, J., Bouchard, N., Ong, H., and De Lean, A. (1995) Stoichiometry of the atrial natriuretic factor-R1 receptor complex in the bovine zona glomerulosa. *Biochemistry 34*, 2130–2136.
10. Larose, L., McNicoll, N., Ong, H., and De Lean, A. (1991) Allosteric modulation by ATP of the bovine adrenal natriuretic factor R1 receptor functions. *Biochemistry 30*, 8990–8995.
11. Duda, T., Venkataraman, V., Ravichandran, S., and Sharma, R. K. (2005) ATP-regulated module (ARM) of the atrial natriuretic factor receptor guanylate cyclase. *Peptides 26*, 969–984.
12. Chinkers, M., and Garbers, D. L. (1989) The protein kinase domain of the ANP receptor is required for signaling. *Science 245*, 1392–1394.
13. Joubert, S., Jossart, C., McNicoll, N., and De Lean, A. (2005) Atrial natriuretic peptide-dependent photolabeling of a regulatory ATP-binding site on the natriuretic peptide receptor-A. *FEBS J. 272*, 5572–5583.
14. Joubert, S., Labrecque, J., and De Lean, A. (2001) Reduced activity of the NPR-A kinase triggers dephosphorylation and homologous desensitization of the receptor. *Biochemistry 40*, 11096–11105.
15. Joubert, S., McNicoll, N., and De Lean, A. (2007) Biochemical and pharmacological characterization of P-site inhibitors on homodimeric guanylyl cyclase domain from natriuretic peptide receptor-A. *Biochem. Pharmacol. 73*, 954–963.
16. Huo, X., Abe, T., and Misono, K. S. (1999) Ligand binding-dependent limited proteolysis of the atrial natriuretic peptide receptor: Juxtamembrane hinge structure essential for transmembrane signal transduction. *Biochemistry 38*, 16941–16951.
17. Labrecque, J., Mc Nicoll, N., Marquis, M., and De Lean, A. (1999) A disulfide-bridged mutant of natriuretic peptide receptor-A displays constitutive activity. Role of receptor dimerization in signal transduction. *J. Biol. Chem. 274*, 9752–9759.
18. Labrecque, J., Deschenes, J., McNicoll, N., and De Lean, A. (2001) Agonistic induction of a covalent dimer in a mutant of natriuretic peptide receptor-A documents a juxtamembrane interaction that accompanies receptor activation. *J. Biol. Chem. 276*, 8064–8072.
19. Parat, M., McNicoll, N., Wilkes, B., Fournier, A., and De Lean, A. (2008) Role of extracellular domain dimerization in agonist-induced activation of natriuretic peptide receptor A. *Mol. Pharmacol. 73*, 431–440.
20. Ogawa, H., Qiu, Y., Ogata, C. M., and Misono, K. S. (2004) Crystal structure of hormone-bound atrial natriuretic peptide receptor extracellular domain: Rotation mechanism for transmembrane signal transduction. *J. Biol. Chem. 279*, 28625–28631.
21. Brown, R. J., Adams, J. J., Pelekanos, R. A., Wan, Y., McKinstry, W. J., Palethorpe, K., Seeber, R. M., Monks, T. A., Eidne, K. A., Parker, M. W., and Waters, M. J. (2005) Model for growth hormone receptor activation based on subunit rotation within a receptor dimer. *Nat. Struct. Mol. Biol. 12*, 814–821.
22. Bell, C. A., Tynan, J. A., Hart, K. C., Meyer, A. N., Robertson, S. C., and Donoghue, D. J. (2000) Rotational coupling of the transmembrane and kinase domains of the Neu receptor tyrosine kinase. *Mol. Biol. Cell 11*, 3589–3599.
23. Moriki, T., Maruyama, H., and Maruyama, I. N. (2001) Activation of preformed EGF receptor dimers by ligand-induced rotation of the transmembrane domain. *J. Mol. Biol. 311*, 1011–1026.
24. Lu, X., Gross, A. W., and Lodish, H. F. (2006) Active conformation of the erythropoietin receptor: Random and cysteine-scanning mutagenesis of the extracellular juxtamembrane and transmembrane domains. *J. Biol. Chem. 281*, 7002–7011.
25. Marquis, M., Fenrick, R., Pedro, L., Bouvier, M., and De Lean, A. (1999) Comparative binding study of rat natriuretic peptide receptor-A. *Mol. Cell. Biochem. 194*, 23–30.
26. Fethiere, J., Meloche, S., Nguyen, T. T., Ong, H., and De Lean, A. (1989) Distinct properties of atrial natriuretic factor receptor subpopulations in epithelial and fibroblast cell lines. *Mol. Pharmacol. 35*, 584–592.
27. Potter, L. R., and Garbers, D. L. (1992) Dephosphorylation of the guanylyl cyclase-A receptor causes desensitization. *J. Biol. Chem. 267*, 14531–14534.
28. Langosch, D., Brosig, B., Kolmar, H., and Fritz, H. J. (1996) Dimerisation of the glycophorin A transmembrane segment in membranes probed with the ToxR transcription activator. *J. Mol. Biol. 263*, 525–530.
29. Kolmar, H., Hennecke, F., Gotze, K., Janzer, B., Vogt, B., Mayer, F., and Fritz, H. J. (1995) Membrane insertion of the bacterial signal transduction protein ToxR and requirements of transcription activation studied by modular replacement of different protein substructures. *EMBO J. 14*, 3895–3904.
30. Brosig, B., and Langosch, D. (1998) The dimerization motif of the glycophorin A transmembrane segment in membranes: Importance of glycine residues. *Protein Sci. 7*, 1052–1056.
31. Sali, A., and Blundell, T. L. (1993) Comparative protein modelling by satisfaction of spatial restraints. *J. Mol. Biol. 234*, 779–815.
32. Bocharov, E. V., Mineev, K. S., Volynsky, P. E., Ermolyuk, Y. S., Tkach, E. N., Sobol, A. G., Chupin, V. V., Kirpichnikov, M. P., Efremov, R. G., and Arseniev, A. S. (2008) Spatial structure of the dimeric transmembrane domain of the growth factor receptor ErbB2 presumably corresponding to the receptor active state. *J. Biol. Chem. 283*, 6950–6956.
33. Poirot, O., Suhre, K., Abergel, C., O'Toole, E., and Notredame, C. (2004) 3DCoffee@igs: A web server for combining sequences and structures into a multiple sequence alignment. *Nucleic Acids Res. 32*, W37–W40.
34. van den Akker, F., Zhang, X., Miyagi, M., Huo, X., Misono, K. S., and Yee, V. C. (2000) Structure of the dimerized hormone-binding domain of a guanylyl-cyclase-coupled receptor. *Nature 406*, 101–104.
35. DeLean, A., Munson, P. J., and Rodbard, D. (1978) Simultaneous analysis of families of sigmoidal curves: Application to bioassay, radioligand assay, and physiological dose-response curves. *Am. J. Physiol. 235*, E97–E102.
36. von Geldern, T. W., Budzik, G. P., Dillon, T. P., Holleman, W. H., Holst, M. A., Kiso, Y., Novosad, E. I., Opgenorth, T. J., Rockway, T. W., and Thomas, A. M.; et al. (1990) Atrial natriuretic peptide antagonists: Biological evaluation and structural correlations. *Mol. Pharmacol. 38*, 771–778.
37. Ottemann, K. M., Xiao, W., Shin, Y. K., and Koshland, D. E., Jr. (1999) A piston model for transmembrane signaling of the aspartate receptor. *Science 285*, 1751–1754.
38. Jiang, G., and Hunter, T. (1999) Receptor signaling: When dimerization is not enough. *Curr. Biol. 9*, R568–R571.
39. Remy, I., Wilson, I. A., and Michnick, S. W. (1999) Erythropoietin receptor activation by a ligand-induced conformation change. *Science 283*, 990–993.
40. Burke, C. L., and Stern, D. F. (1998) Activation of Neu (ErbB-2) mediated by disulfide bond-induced dimerization reveals a receptor tyrosine kinase dimer interface. *Mol. Cell. Biol. 18*, 5371–5379.
41. Livnah, O., Johnson, D. L., Stura, E. A., Farrell, F. X., Barbone, F. P., You, Y., Liu, K. D., Goldsmith, M. A., He, W., Krause, C. D., Pestka, S., Jolliffe, L. K., and Wilson, I. A. (1998) An antagonist peptide-EPO receptor complex suggests that receptor dimerization is not sufficient for activation. *Nat. Struct. Biol. 5*, 993–1004.
42. Chinkers, M., and Wilson, E. M. (1992) Ligand-independent oligomerization of natriuretic peptide receptors. Identification of heteromeric receptors and a dominant negative mutant. *J. Biol. Chem. 267*, 18589–18597.
43. Carpenter, K. A., Wilkes, B. C., De Lean, A., Fournier, A., and Schiller, P. W. (1997) Hydrophobic forces are responsible for the folding of a highly potent natriuretic peptide analogue at a membrane mimetic surface: An NMR study. *Biopolymers 42*, 37–48.
44. Kobilka, B. K., and Deupi, X. (2007) Conformational complexity of G-protein-coupled receptors. *Trends Pharmacol. Sci. 28*, 397–406.